Entanglement generation between spinor Bose-Einstein condensates using Rydberg excitations

Idlas, S.; Domenzain, L.; Spreeuw, R.J.C.; Byrnes, T.

Published in:
Physical Review A - Atomic, Molecular, and Optical Physics

DOI:
10.1103/PhysRevA.93.022319

Entanglement generation between spinor Bose-Einstein condensates using Rydberg excitations

Sandrine Idlas,[1,2,3] Luis Domenzain,[2,4] Robert Spreeuw,[5] and Tim Byrnes[1,2,6]
[1]*New York University, 1555 Century Avenue, Pudong, Shanghai 200122, China*
[2]*National Institute of Informatics, 2-1-2 Hitotsubashi, Chiyoda-ku, Tokyo 101-8430, Japan*
[3]*KTH, Royal Institute of Technology, Stockholm, Sweden*
[4]*Université Pierre et Marie Curie (Paris VI), Sorbonne Universités*
[5]*Van der Waals-Zeeman Instituut, Universiteit van Amsterdam, P.O. Box 94485 1090 GL Amsterdam, The Netherlands*
[6]*NYU-ECNU Institute of Physics at NYU Shanghai, 3663 Zhongshan Road North, Shanghai 200062, China*
(Received 20 November 2015; revised manuscript received 13 January 2016; published 12 February 2016)

We propose an experimental scheme of generating entangled states between two spinor Bose-Einstein condensates (BECs) using Rydberg excitations. Due to the strong interaction between Rydberg atoms, the Rydberg excitation creates an interaction between two closely located BECs. The method is suitable particularly for atom chip and permanent magnetic trap systems, which can create many BECs with an arbitrary two-dimensional geometry. We show two schemes of entangled state generation, based on stimulated Raman adiabatic passage (STIRAP) methods. The first method produces a symmetric state with total S^x spin zero between ground and excited states of the atoms using a single STIRAP pair, while the second produces a NOON state between hyperfine ground states using two STIRAP pairs. We show that despite the additional complexity of the BECs, it is possible to identify the initial and final adiabatic states exactly. We verify our theoretical predictions using numerical simulations on small boson number systems.

DOI: 10.1103/PhysRevA.93.022319

I. INTRODUCTION

Entanglement is now understood to be one of the unique features of quantum mechanics and is a key ingredient to quantum information tasks that provide speedups over its classical counterpart [1]. The controlled creation of entanglement is now routinely achievable in the laboratory in a great variety of different systems, including trapped ions, superconducting circuits, photons, quantum dots, and nitrogen-vacancy (NV) centers in diamond [2–7]. Typically the systems where controlled entanglement is producible are microscopic, single-particle systems. While it is natural to expect that quantum behavior is more apparent in microscopic systems due to the larger energy scale of quantum effects for small systems, some macroscopic systems have also been demonstrated to possess entanglement. One notable example is using atomic ensembles, where entanglement was produced between two ensembles by interacting coherent light with them [8]. This technique was used to realize teleportation between the ensembles [9]. Several other examples showing entanglement between macroscopic ensembles have also been realized [10].

Meanwhile, there has recently been great advances in the ability to create and control atomic Bose-Einstein condensates (BECs). This involves not only the ability to trap BECs in a variety of different geometries and thereby controlling their spatial wave function [11], but also control the internal states of the atoms [12–14]. The control of the internal states of the BEC have been achieved in optical dipole traps as well as in magnetic traps, but also on atom chips, which allow for a compact platform for forming and controlling BECs. A particularly promising platform for BECs is the use of permanent magnetic traps to create BECs [15–19]. In this approach, trapping centers, made of a material such as FePt [4], are patterned to create a desired two-dimensional geometry. The atom chip and permanent magnetic trap approach make it an ideal platform for creating multiple BECs located in close proximity to each other. This opens the possibility of creating entanglement between two BECs. Several theoretical proposals to achieve this have been investigated such as schemes involving those using atomic interactions [20,21], entanglement of many distant BECs in an optical lattice by interference [22], and entanglement in quantum network of BECs [17,23,24]. Entanglement generation in BECs has applications for quantum computing and quantum metrology [13,21–23,25–27]. For quantum computation, two hyperfine levels of the atoms in the BEC can be used as qubit states to encode information. It is possible to create arbitrary superpositions of the two components of the BEC and to manipulate them in the same way as standard qubits [24,28–30].

In this paper we introduce a method of entangling two BECs using Rydberg excitations. A Rydberg atom is an atom with one or more electrons with a very high principal quantum number n. One of the characteristic features of the Rydberg is that is that it has an extremely large Bohr radius. For an electron in a Rydberg state corresponding to $n = 100$, the diameter of the atom is typically several hundred nanometers. For separations of 5–10 μm between two Rydberg atoms, the dominant interaction is a long-range dipole-dipole interaction due to the Rydberg excitation. At this distance, other interactions, such as interactions between atoms in the ground state and a Rydberg atom, or interactions between two ground states atoms, are negligible [31]. When a Rydberg excitation is present, this results in a shift of the energy levels of the surrounding atoms, so that the Rydberg state is off-resonant with the excitation laser and therefore not accessible, resulting in a Rydberg blockade. In the context of a BEC, if the energy level of the Rydberg atom is high enough in a Bose-Einstein condensate, all other states containing more than one Rydberg excitation can be ignored [32,33]. In the case of permanent magnetic traps, the trapping centers can be patterned to have a lattice period of <10 μm, making them suitable for generating

entanglement with Rydberg excitations. We take advantage of this Rydberg blockade between two BECs to produce entanglement between the internal states of the BECs.

A scheme to entangle two atoms using the Rydberg blockade was previously developed in Refs. [3,6]. The procedure is to use a STIRAP (stimulated Raman adiabatic passage) to adiabatically create a Rydberg excitation in both of the atoms. This can be used as the basis of an entangling gate in two ways. In the first scheme, when the two Rydberg excitations are both excited, there is a blockade due to the high-energy penalty of having two Rydberg states. This "pushes" both of the excitations out of the Rydberg state and an entangled state is created between the initial ground state and the intermediate excited state. In the second scheme, a second STIRAP sequence is used to reverse the effect of the first STIRAP sequence. This results in a geometric phase that can be used as the basis of an entangling gate. For the BEC case, the situation is considerably more complex due to the larger Hilbert space involved for BECs. In this paper, we show that it is possible to adapt this scheme and show exactly the adiabatic initial and final states for the STIRAP process. We perform some numerical calculations to verify the agreement to the theory.

The rest of this paper is organized as follows. In Sec. II, we first describe the single-STIRAP entangling schemes developed in Refs. [34,35], which will lead to developing a scheme to entangle two Bose-Einstein condensates. We confirm our predictions using numerical results. In Sec. III, we discuss the double-STIRAP geometric phase gate entangling scheme, first for the atomic case and then we generalize to BECs. We again show numerical results to verify our predictions. We summarize our findings in Sec. IV and discuss future prospects.

II. SINGLE-STIRAP ENTANGLED STATE GENERATION

In this section we discuss a method for generating entanglement between two systems using an adiabatic transition and Rydberg excitations. We first consider for simplicity the case for qubits, then generalize to two BECs. The form of the entanglement that is generated is total spin-zero state in the S^x basis, where N is the number of atoms in the BEC.

A. Qubit case

Let us first review a method of entangling two atoms via a Rydberg excitation, following Refs. [34,35]. This will serve as a starting point for generalizing the method for entangling two BECs. The energy levels involved in the scheme are shown in Fig. 1(a). The atoms are initially assumed to be in the ground state g_i, where $i = 1, 2$ is the atom index. Another f_i is an auxiliary state that is unused for this scheme, this will be used in Sec. III. The Rydberg states r_i are excited through an intermediate state e_i. A possible choice for the levels g_i and e_i could be the hyperfine ground states of ^{87}Rb. The $5p$ state of ^{87}Rb would not be a good candidate as an e_i state, because it is a short-lived state. The e_i-r_i transition may also be a two-photon Rydberg excitation, where a large intermediate state detuning with respect to the intermediate $5p$ state is used.

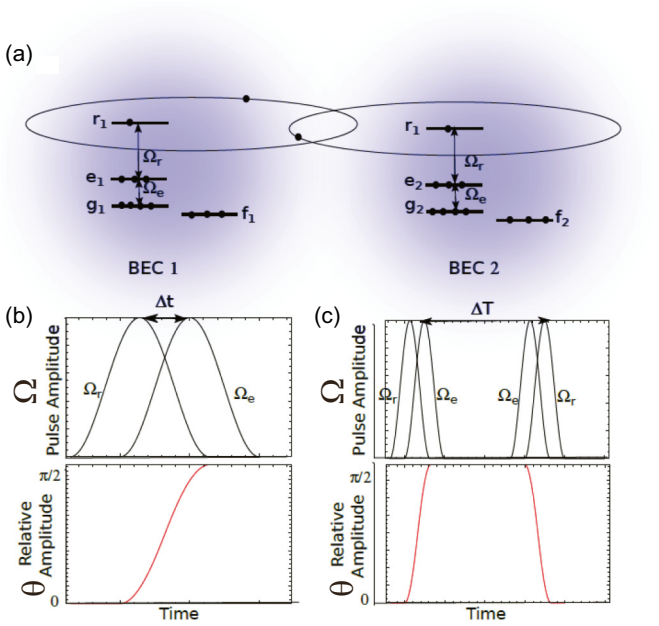

FIG. 1. (a) Representation of the energy levels used for the STIRAP schemes. g_i and f_i are the energy levels of the ground states of the atoms forming the BECs for $i = 1, 2$. e_i are the energy levels for the excited states, and r_i are the Rydberg levels. (b) Pulses for the STIRAP sequence. The pulses are in counterintuitive order: the sequence starts with the pulse coupling the unpopulated states $|e_i\rangle$ and $|r_i\rangle$, not affecting the initial state until the pulse coupling the states $|e_i\rangle$ and $|g_i\rangle$ is turned on. (c) Pulses for the two-STIRAP sequences. The second pulse sequence is in reverse order compared to the first one. The relative amplitude $\tan\theta = |\frac{\Omega_e}{\Omega_r}|$ is also plotted for the one- and two-STIRAP sequences.

The Hamiltonian for the system can be written

$$H = H_r + H_e + U|r_1\rangle|r_2\rangle\langle r_1|\langle r_2|, \tag{1}$$

$$H_r = \hbar\sum_{i=1}^{2}(\Omega_r(t)|e_i\rangle\langle r_i| + \Omega_r^*(t)|r_i\rangle\langle e_i|), \tag{2}$$

$$H_e = \hbar\sum_{i=1}^{2}(\Omega_e(t)|e_i\rangle\langle g_i| + \Omega_e^*(t)|g_i\rangle\langle e_i|), \tag{3}$$

where Ω_r is the Rabi frequency between the excited and Rydberg states, Ω_e the Rabi frequency between the ground and excited states, and U is the energy between two Rydberg atoms due to the dipole-dipole interaction. The interaction is long ranged, which allows for the atoms to be separated by several microns and yet have a significant interaction.

1. Independent atom case $U = 0$

In the absence of the dipole-dipole interactions ($U = 0$), the transitions are two independent Ξ systems, which possess a dark state (eigenstate with zero energy),

$$|D_i(\theta)\rangle = \cos\theta|g_i\rangle - \sin\theta e^{i\phi(t)}|r_i\rangle. \tag{4}$$

Here we have parameterized

$$\Omega_e(t) = A_e(t), \tag{5}$$

$$\Omega_r(t) = A_r(t)e^{-i\phi(t)}, \tag{6}$$

where the relative amplitude is

$$\tan\theta = \frac{A_e(t)}{A_r(t)}. \tag{7}$$

Here $\phi(t)$ is the relative phase between the two pulses, which may be time varying. An elementary example of such a time-dependent phase is $\phi(t) = \omega t$, where ω is the detuning. The state Eq. (4) forms the basis of adiabatically exciting a Rydberg state from the ground state. This can be performed by preparing the atom in the ground state $|g_i\rangle$, then gradually changing the amplitude of the transitions such that it begins with $\theta = 0$ and ends with $\theta = \pi/2$. By doing so the ground state is adiabatically changed from $|g_i\rangle$ to $|r_i\rangle$. This may be conveniently achieved in practice by two pulses that are staggered in time in the so-called "counterintuitive" sequence, where H_r is applied first, as shown in Fig. 1(b).

2. *Atoms coupled with Rydberg interaction*

With the interactions U turned on, the Hamiltonian Eq. (1) still possesses two dark states, written as

$$\begin{aligned}|D_+(\theta)\rangle &= \frac{1}{\sqrt{\cos^4\theta + 2\sin^4\theta}}[\cos 2\theta\,|g_1\rangle\,|g_2\rangle + \sin^2\theta\,|e_1\rangle\,|e_2\rangle \\ &\quad - e^{i\phi(t)}\cos\theta\sin\theta(|g_1\rangle\,|r_2\rangle + |r_1\rangle\,|g_2\rangle)], \\ |D_-(\theta)\rangle &= \frac{1}{\sqrt{2}}[\sin\theta(|e_1\rangle|g_2\rangle - |g_1\rangle|e_2\rangle) \\ &\quad + e^{i\phi(t)}\cos\theta(|e_1\rangle|r_2\rangle - |r_1\rangle|e_2\rangle)].\end{aligned} \tag{8}$$

The first state is symmetric under interchange of the atoms, the second is antisymmetric. Due to the energy penalty U of the $|r_1\rangle|r_2\rangle$ state, the dark state $|D_\pm\rangle$ no longer involves this state. This is in contrast to the independent case Eq. (4), where $|D_1\rangle|D_2\rangle$ involves the double Rydberg state.

Let us consider the case where we start in the state $|g_1\rangle|g_2\rangle$ and then impart the same adiabatic procedure as before. Only $|D_+\rangle$ contains the initial state as it is symmetric under interchange of particles, hence this is the relevant state. Considering $\phi(t) = 0$ for simplicity, and examining the limiting cases starting from $\theta = 0$ and evolving to $\theta = \pi/2$, we may deduce that

$$|g_1\rangle|g_2\rangle \to \frac{1}{\sqrt{2}}(|e_1\rangle\,|e_2\rangle - |g_1\rangle\,|g_2\rangle). \tag{9}$$

This is a maximally entangled state in the states $|g_i\rangle$ and $|e_i\rangle$. Thus, while for $U = 0$ the STIRAP sequence produces no entanglement, in this case it directly creates an entangled state.

We may derive the adiabatic transition Eq. (9) in a simple way that does not require explicit diagonalization of the Hamiltonian Eq. (1). Let us write Eq. (3) as

$$H_e = \hbar A_e(t)\left(\sigma_1^x + \sigma_2^x\right), \tag{10}$$

where

$$\sigma_i^x = |e_i\rangle\langle g_i| + |g_i\rangle\langle e_i|. \tag{11}$$

By the definition of the dark state, the final state after the STIRAP pulses is the zero-energy state with only H_e present. Thus, we may find the final state by finding the zero-energy state of H_e, which has two solutions:

$$\begin{aligned}|+\rangle|-\rangle &= \tfrac{1}{2}(|g_1\rangle + |e_1\rangle)(|g_2\rangle - |e_2\rangle), \\ |-\rangle|+\rangle &= \tfrac{1}{2}(|g_1\rangle - |e_1\rangle)(|g_2\rangle + |e_2\rangle).\end{aligned} \tag{12}$$

Again due to the symmetry under interchange of atoms $1 \leftrightarrow 2$, the final state must also obey this symmetry as the initial state is symmetric and the Hamiltonian itself is also symmetric. This gives the state

$$\begin{aligned}|D_+(\theta = \pi/2)\rangle &= \frac{1}{\sqrt{2}}(|+\rangle|-\rangle + |-\rangle|+\rangle) \\ &= \frac{1}{\sqrt{2}}(|e_1\rangle\,|e_2\rangle - |g_1\rangle\,|g_2\rangle).\end{aligned} \tag{13}$$

This is the same final state as Eq. (9), which is a maximally entangled Bell state.

B. Generalizing to the BEC case

We now generalize the entanglement scheme of the previous section to the BEC case. We assume that the spatial degrees of freedom of the BEC are completely in the ground state of the traps, so that they do not play any role in the subsequent dynamics. The only degrees of freedom are then which levels are occupied in Fig. 1. We also assume that each BEC contains a fixed number of atoms, denoted N_i. Due to the Rydberg blockade, we assume that Rydberg excitation can be occupied by only one atom. The Hilbert space is therefore spanned by the states

$$|k_i,\sigma_i\rangle_z = \begin{cases} \frac{1}{\sqrt{k_i!(N_i-k_i)!}}(g_i^\dagger)^{k_i}(e_i^\dagger)^{N_i-k_i}|0\rangle & \text{if } \sigma_i = 0 \\ \frac{1}{\sqrt{k_i!(N_i-k_i-1)!}}(g_i^\dagger)^{k_i}(e_i^\dagger)^{N_i-k_i-1}|r_i\rangle & \text{if } \sigma_i = r \end{cases}, \tag{14}$$

where $g_i^\dagger, e_i^\dagger$ are the bosonic creation operators for the g_i, e_i levels, respectively, $\sigma_i = 0, r_i$ represents either the absence or presence of the Rydberg excitation, respectively, and $i = 1, 2$ labels each of the BECs. The Hamiltonian can now be straightforwardly adapted to the BEC case,

$$H = H_e + H_r + U|r_1\rangle|r_2\rangle\langle r_1|\langle r_2|, \tag{15}$$

$$H_r = \hbar\sum_{i=1}^{2}(\Omega_r(t)\sigma_i^- e_i^\dagger + \Omega_r^*(t)\sigma_i^+ e_i), \tag{16}$$

$$H_e = \hbar\sum_{i=1}^{2}(\Omega_e(t)e_i^\dagger g_i + \Omega_e^*(t)g_i^\dagger e_i), \tag{17}$$

where as before $\Omega_{e,r}(t)$ is the Rabi frequency between the $g_i \leftrightarrow e_i$ and $e_i \leftrightarrow r_i$ states, respectively, and U is the long-ranged dipole-dipole interaction between the Rydberg states.

1. *Independent BEC case $U = 0$*

Let us again first consider the case $U = 0$, so that the two BECs are completely decoupled. Due to the multibosonic nature of the problem, it is nontrivial to write down a general expression for the dark states. It is possible to write an

expression for some small boson numbers $N_i = 2, 3$,

$$|D_i(\theta); N_i = 2\rangle \propto -\frac{\cos 2\theta}{\sqrt{2}}|2,0\rangle_z + \cos\theta \sin\theta |1,r_i\rangle_z - \frac{\sin^2\theta}{\sqrt{2}}|0,0\rangle_z, \quad (18)$$

$$|D_i(\theta); N_i = 3\rangle \propto -\frac{\cos 3\theta}{\sqrt{3}}|3,0\rangle_z + \cos 2\theta \sin\theta |2,r_i\rangle_z - \cos\theta \sin^2\theta |1,0\rangle_z + \sin^3\theta |0,r_i\rangle_z, \quad (19)$$

where we have set the relative phase ϕ between the pulses to zero for simplicity, and we have omitted normalization constants. Adiabatically evolving the pulses such that the relative amplitudes are changed starting from $\theta = 0$ to $\theta = \pi/2$, this induces the transitions

$$|2,0\rangle_z \to \frac{1}{\sqrt{2}}(|2,0\rangle_z - |0,0\rangle_z) \quad N = 2, \quad (20)$$

$$|3,0\rangle_z \to \frac{1}{\sqrt{2}}(|2,r_i\rangle_z - |0,r_i\rangle_z) \quad N = 3. \quad (21)$$

The transition Eqs. (20) and (21) again can be deduced in a simple way following the same reasoning as the previous section. Initially, $\theta = 0$, hence $\Omega_e = 0$ and only H_r is present. As discussed in Ref. [34], the only zero-energy state is when there is no population in level e_i or r_i. This means that all the population must be present in the g_i state, and the zero-energy state is $|N_i,0\rangle$. At the end of the adiabatic evolution $\theta = \pi/2$, and therefore only H_e is present. The Hamiltonian on each BEC is then

$$H_e^{(i)} = \hbar A_e(t) S_i^x, \quad (22)$$

where $S_i^x = g_i^\dagger e_i + e_i^\dagger g_i$. As the interactions U are off, the two BECs are completely decoupled and the dark states are therefore simply a zero eigenvalue eigenstate of S_i^x, separately. In general, the eigenstates of S_i^x can be written

$$|k_i,\sigma_i\rangle_x = \begin{cases} \frac{1}{\sqrt{k_i!(N_i-k_i)!}}(g_{x,i}^\dagger)^{k_i}(e_{x,i}^\dagger)^{N_i-k_i}|0\rangle & \text{if } \sigma_i = 0 \\ \frac{1}{\sqrt{k_i!(N_i-k_i-1)!}}(g_{x,i}^\dagger)^{k_i}(e_{x,i}^\dagger)^{N_i-k_i-1}|r_i\rangle & \text{if } \sigma_i = r \end{cases}, \quad (23)$$

where k_i^x is an integer between 0 and N_i inclusive and the eigenvalue is $2k_i^x - N_i$. Here,

$$g_{x,i}^\dagger = \frac{1}{\sqrt{2}}(g_i^\dagger + e_i^\dagger),$$
$$e_{x,i}^\dagger = \frac{1}{\sqrt{2}}(g_i^\dagger - e_i^\dagger). \quad (24)$$

If N_i is even, the zero-energy eigenstates are simply $|k_i^x = N_i/2\rangle$. On the other hand, if N_i is odd, there is no zero eigenvalue state of S_i^x. As suggested by Eq. (21), the zero energy eigenstate is in this case that with one Rydberg excitation, which then makes the number of atoms in the g_i and e_i levels even. We may thus infer that in general the adiabatic evolution induces the transition [34]

$$|N_i,0\rangle_z \to \begin{cases} \left|k_i = \frac{N_i}{2},0\right\rangle_x & \text{if } N \text{ even}, \\ \left|k_i = \frac{N_i-1}{2},r_i\right\rangle_x & \text{if } N \text{ odd}. \end{cases} \quad (25)$$

One may easily evaluate that the above reduces to the specific case shown in Eq. (21) for $N_i = 2, 3$. The odd or even effect is caused by the fact that the zero eigenvalues of S_i^x are $2k_i^x - N = 0$. This implies that N needs to be an even number for the eigenvalue to be zero. When it is an odd number, a way to obtain a zero eigenstate is to occupy a Rydberg level, as $N - 1$ is then even.

Due to the odd or even effect shown in Eq. (25) (originally given in Ref. [34]), we note that the above sequence could be potentially used to detect parity without having to count the actual number of particles. In this case the scheme would run as in Fig. 1(c), where there are two STIRAP pairs, first to detect a Rydberg excitation, then the sequence would be reversed to return the atoms to their original state. As the state obtained after the first STIRAP transition depends on the parity of the Bose-Einstein condensate, determining the presence of a Rydberg excitation before reversing the transition back would be equivalent to determining the parity. A novel sensitive technique to detect Rydberg atoms, which uses the strong interaction among Rydberg atoms to enhance the imaging sensitivity, has recently been proposed theoretically and demonstrated experimentally [36,37]. The parity dependence of the result in Eq. (25) indicates that this can also be used to prepare an ensemble with definite even parity in the number of atoms. For this application, one would remove the Rydberg atom, for example by ionizing it. The effectiveness of this is would depend on the level of adiabaticity, and whether there are any "dark" atoms, which do not respond to the STIRAP process, due to thermal excitations and other imperfections.

2. *BECs coupled with Rydberg interaction*

Now let us introduce the interaction U, which couples the two BECs. It is again a nontrivial problem to find an exact expression for the dark states. For this reason we have numerically found the eigenstates of the Hamiltonian Eq. (15) for a range of parameters. For simplicity we shall consider the case where there are equal numbers of atoms in each BEC $N_1 = N_2 = N$, although we show generalizations of this in Sec. III. Some typical results are shown in Fig. 2. We see that there are generally two energy branches, one centered around zero energy and another around the Rydberg excitation energy U. In what we consider, we assume that the initial state is $|N,0\rangle|N,0\rangle$, i.e., the state with all atoms in the state g_i. This is a zero-energy state at the beginning of the evolution of Fig. 2. Thus, we are interested in energy eigenstates that have zero energy for the entire evolution. For all parameters and boson numbers N we were able to find two zero-energy dark states, corresponding to the symmetric and antisymmetric solutions with respect to interchange of BECs, in a similar way to the single atom case, Eq. (8). As the initial state is symmetric under interchange of BECs, the relevant dark state is the symmetric solution; thus, there is a unique state that transfers the initial state from $|N,0\rangle|N,0\rangle$ to a final zero-energy state.

Despite the difficulty of finding an explicit expression for the dark state, we may use a similar technique to that used in the previous section to find the final entangled state. At the end of the adiabatic evolution, only the Hamiltonian Eq. (17) is present, which may be written

$$H_e = \hbar A_e(t)\left(S_1^x + S_2^x\right). \quad (26)$$

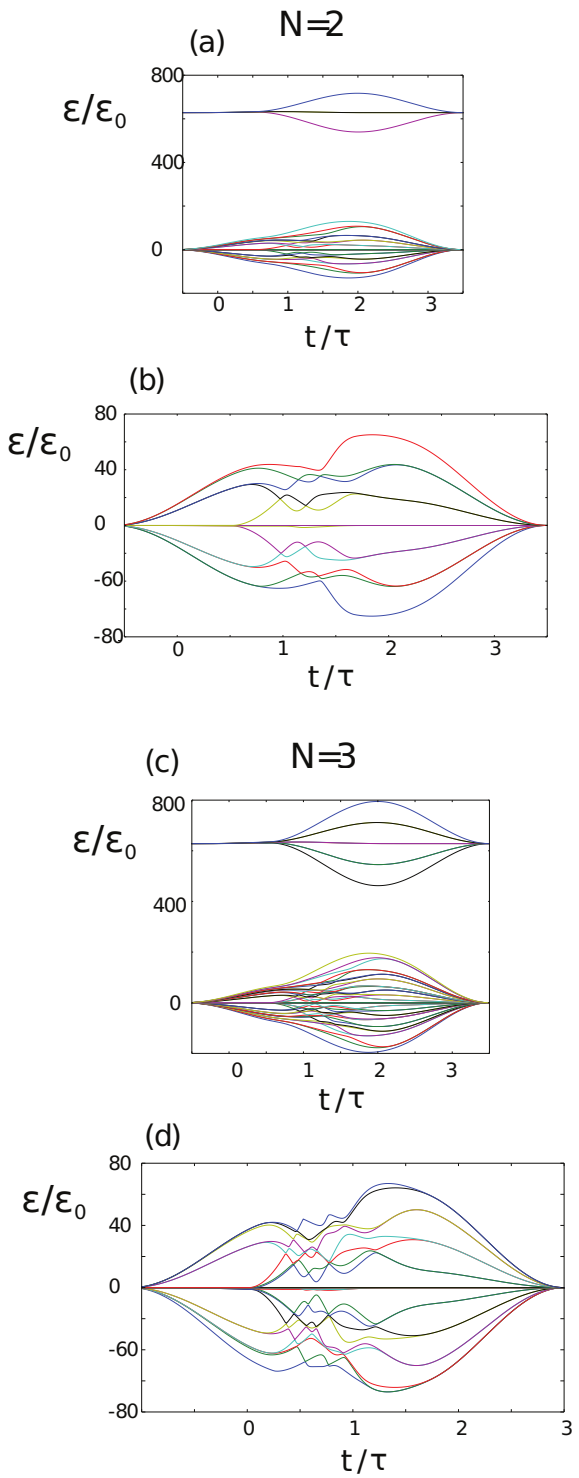

FIG. 2. Energy eigenvalues ε of the Hamiltonian Eq. (15) for (a, b) $N_1 = N_2 = 2$ and (c, d) $N_1 = N_2 = 3$. (b) and (d) are zoomed in versions of (a) and (c) near the zero-energy region. We use pulses for $\Omega_{e,r}$ as defined in Eqs. (30) and (31). Parameters used are $\epsilon_0 = \hbar/\tau$, $\Delta t/\tau = 0.11$, $\Omega_r^{\max}\tau = 500\pi$, $\Omega_e^{\max}\tau = 500\pi$, and $U\tau/\hbar = 200\pi$.

We seek the zero-energy eigenstates of this Hamiltonian, which are $|k,0\rangle_x|N-k,0\rangle_x$, where $k \in \{0,N\}$. Note that we may safely assume there is no Rydberg excitation as the total number of atoms here is $2N$ in this case. In general, any superposition of these states also is a zero eigenvalue state, thus a candidate state for the final state is

$$\sum_{k=0}^{N} \xi_k |k,0\rangle_x |N-k,0\rangle_x. \tag{27}$$

However, much like the qubit case discussed above, due to the symmetric nature of the Hamiltonian Eq. (15) and the initial state, the state must also be a symmetric state under interchange of BECs. This imposes the restriction that $\xi_k = \xi_{N-k}$ but still does not fix all the coefficients. Despite the generality of the state, the symmetrization guarantees that the final state is entangled, this implies that there must be at least two values of ξ_k, which are nonzero. For example, for the particular case that only ξ_0 and ξ_N are nonzero, we have the state

$$\frac{1}{\sqrt{2}}[|N,0\rangle_x|0,0\rangle_x + |0,0\rangle_x|N,0\rangle_x]. \tag{28}$$

Ignoring the Rydberg labels, which are all unoccupied, this is a NOON state in the S^x basis, which is a type of Bell state involving macroscopic states. Quantifying the entanglement with the logarithmic negativity, this has an entanglement $E = 1$, which is in fact a minimally entangled state within the possibilities allowed in Eq. (27). A maximally entangled state would have $|\xi_k| = 1/\sqrt{N+1}$, and has an entanglement equal to $E_{\max} = \log_2(N+1)$ [38].

C. Numerical analysis

In the previous sections we showed that there should be a zero-energy dark state that is suitable for adiabatic evolution. As is true for any adiabatic process, the Hamiltonian must be time evolved slowly enough such that the state remains in the same energetic state. This is best demonstrated by an explicit evolution of the dynamical system. To this end, we propagate the time-dependent Schrödinger equation in the basis specified by Eq. (14) using the fourth-order Runge-Kutta method. We time-evolve the equation

$$i\hbar\frac{d\psi_{\boldsymbol{n}}}{dt} = \sum_{\boldsymbol{n}'} H_{\boldsymbol{n}\boldsymbol{n}'}\psi_{\boldsymbol{n}'}, \tag{29}$$

where $\boldsymbol{n} = \{k_1,\sigma_1,k_2,\sigma_2\}$ and $\boldsymbol{n}' = \{k_1',\sigma_1',k_2',\sigma_2'\}$, and $H_{\boldsymbol{n}\boldsymbol{n}'} = \langle k_1\sigma_1|_z\langle k_2\sigma_2|_z H |k_1'\sigma_1'\rangle_z|k_2'\sigma_2'\rangle_z$ with H defined in Eq. (15). $\psi_{\boldsymbol{n}} = \langle k_1\sigma_1|_z\langle k_2\sigma_2|_z|\psi(t)\rangle$, where $|\psi(t)\rangle$ is the evolved state at time t. We use pulse shapes according to the "counterintuitive" sequence defined by

$$\Omega_e(t) = \begin{cases} \Omega_e^{\max}\sin^2\left(\frac{\pi t}{\tau}\right) & 0 < t < \tau \\ 0 & \text{otherwise,} \end{cases} \tag{30}$$

$$\Omega_r(t) = \begin{cases} \Omega_r^{\max}\sin^2\left(\frac{\pi(t+\Delta t)}{\tau}\right) & -\Delta t < t < \tau - \Delta t \\ 0 & \text{otherwise,} \end{cases} \tag{31}$$

where τ is the pulse duration, $\Delta t > 0$ is the delay between the pulses, and $\Omega_{e,r}^{\max}$ are the maximum amplitudes of the pulses. The states are initialized such that

$$\psi_{k_1\sigma_1k_2\sigma_2} = \delta_{k_1,N}\delta_{\sigma_1,0}\delta_{k_2,N}\delta_{\sigma_2,0}, \tag{32}$$

where $\delta_{n,m}$ is the Kronecker δ.

Figure 3 shows typical results for the probability of occupation $|\psi_{\boldsymbol{n}}|^2$ of each of the basis states as the Schrödinger equation is evolved. The adiabatic limit can be reached in one of two ways. The first way is to keep $\Omega_{r,e}^{\max}$ fixed and

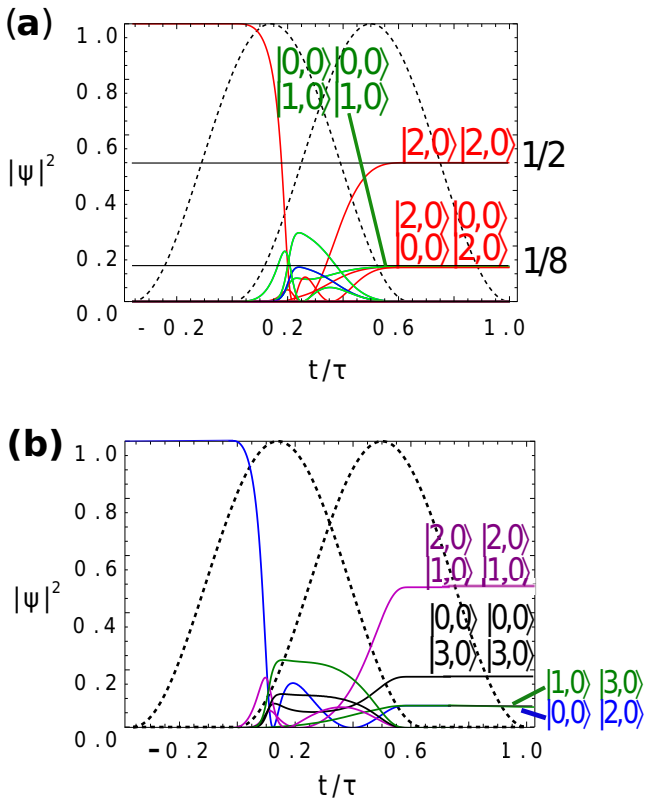

FIG. 3. Probability amplitude $|\psi_{\boldsymbol{n}}|^2$ evolution during the STIRAP sequence for states $|k_1, k_2, r_1, r_2\rangle$ with (a) $N = 2$ and (b) $N = 3$. In (a), horizontal lines show populations of labeled states in the ideal adiabatic case. Parameters used are (a) $\Delta t/\tau = 0.36$, $\Omega_r^{\max}\tau = 60\pi$, $\Omega_e^{\max}\tau = 60\pi$, $U\tau/\hbar = 200\pi$; (b) $\Delta t/\tau = 0.36$, $\Omega_r^{\max}\tau = 10^4$, $\Omega_e^{\max}\tau = 10^4$, $U\tau/\hbar = 2\Omega_r^{\max}$.

make the timescale τ of the pulses long enough such that the state follows an adiabatic path. Alternatively, for a fixed pulse duration τ, the pulse amplitudes $\Omega_{r,e}^{\max}$ should be large enough. These are strictly equivalent as can be considered by examining the dimensionless parameters in the problem, which are $\Omega_{r,e}^{\max}\tau$, $\Delta t/\tau$, and $U\tau/\hbar$. While in our simulations there is no restriction of the $\Omega_{r,e}^{\max}$, U, τ that can be chosen, in an experimental situation the Rydberg blockade is not an *in situ* controllable parameter, hence this gives a practical constraint to what the other parameters can take. In order that the Rydberg blockade regime is achieved, one should have $U \gtrsim \hbar\Omega_{r,e}$, which limits the strength of the pulses. Thus, then to achieve adiabaticity under this constraint, one must increase τ to sufficiently long times.

The probability amplitudes of the numerically evolved states according to the above are shown in Fig. 3(a). We find that in the case of $N = 2$ the evolved state is

$$\begin{aligned}|\mathrm{NOON}, N = 2\rangle &= \frac{1}{\sqrt{2}}(|2,0\rangle_x|0,0\rangle_x + |0,0\rangle_x|2,0\rangle_x) \\ &= \frac{1}{\sqrt{8}}(|0,0\rangle_z|0,0\rangle_z + |2,0\rangle_z|0,0\rangle_z \\ &\quad + |0,0\rangle_z|2,0\rangle_z + |2,0\rangle_z|2,0\rangle_z) - \frac{1}{\sqrt{2}}|1,0\rangle_z|1,0\rangle_z, \quad (33)\end{aligned}$$

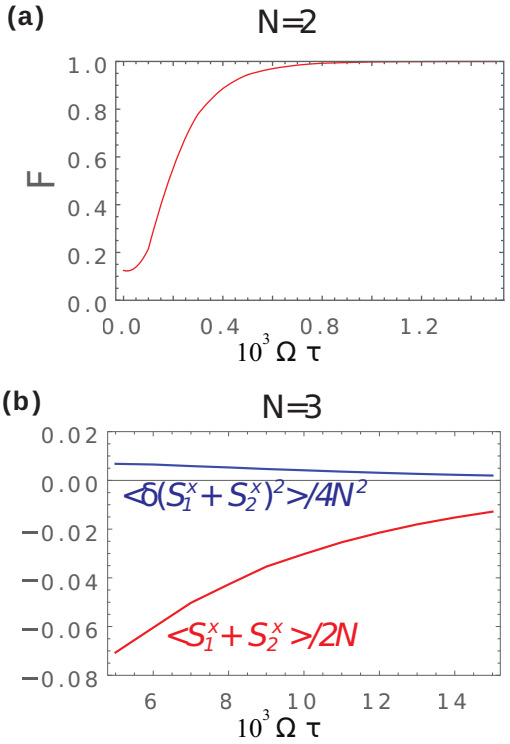

FIG. 4. Fidelity of the final state after adiabatic evolution with respect to the ideal NOON state Eq. (28). Particle numbers correspond to (a) $N = 2$ and (b) $N = 3$. Parameters used are $\Delta t/\tau = 0.36$, $\Omega_r^{\max} = \Omega_e^{\max} = \Omega$, and $U\tau/\hbar = 2\Omega$.

which corresponds to a NOON state Eq. (28) with $N = 2$. Comparing the probability amplitudes of the NOON state in the z basis with the numerical results, we see that there is good agreement with the final values after the adiabatic evolution. To examine the effectiveness of the adiabatic evolution we examine the fidelity,

$$F = |\langle \mathrm{NOON}, N = 2|\psi(t = \tau)\rangle|^2, \quad (34)$$

of the final states Eq. (33) with the numerically evolved state. Figure 4(a) shows that the fidelity approaches 1 as expected, as when $\Omega^{\max}$ is increased this improves the adiabaticity of the STIRAP pulses. For strong pulses (or equivalently long pulse durations) we obtain the NOON state with very high fidelity.

For the $N = 3$ case, we do not see that the state approaches a NOON state, hence this appears to be a special case for $N = 2$. The state is found to agree with the general form of Eq. (27). This state should have the properties of having zero expectation value with respect to the Hamiltonian Eq. (26),

$$\left\langle \left(S_1^x + S_2^x\right)\right\rangle = 0, \quad (35)$$

and be an eigenstate of Eq. (26), meaning that

$$\left\langle \delta\left(S_1^x + S_2^x\right)^2\right\rangle = \left\langle \left(S_1^x + S_2^x\right)^2\right\rangle - \left\langle \left(S_1^x + S_2^x\right)\right\rangle^2 = 0. \quad (36)$$

Figure 4(b) shows the expectation value and variance as a function of $\Omega^{\max}$. We see that these approach the expected value of 0 as the pulse amplitudes are increased, in a similar way to Fig. 4(a), due to the increased adiabaticity. We find that as N is increased it becomes more difficult to achieve adiabaticity, requiring larger values of $\Omega_{r,e}^{\max}\tau$. This will be one

of the limitations when trying to achieve entangled BEC states with large N. This is due to the fact that in the nonadiabatic regime, the process is uncontrolled and can generate a different state involving more states in the superposition, which would lead to more entanglement.

To directly observe entanglement in the final state, we calculated the logarithmic negativity of the final state after the adiabatic evolution. Due to deviations from perfect adiabaticity, our final state involves in general a finite population of Rydberg states, which will have the effect of reducing the entanglement. We treat this by tracing out these degrees of freedom to obtain a density matrix in the space of $|k_1,k_2\rangle$:

$$\rho = \mathrm{Tr}_{r_1,r_2}|\psi\rangle\langle\psi| = \sum_{\sigma_1\sigma_2}\langle\sigma_1|\langle\sigma_2|\psi\rangle\langle\psi|\sigma_1\rangle|\sigma_2\rangle. \tag{37}$$

The logarithmic negativity is then calculated by evaluating

$$E = \log_2 ||\rho^{T_2}|| = \log_2 \sum_i |\lambda_i|, \tag{38}$$

where ρ^{T_2} is the partial transpose of ρ with respect to BEC 2, and $||\cdot||$ is the trace norm of a matrix. The last form of Eq. (38) shows the most suitable form for evaluation, where λ_i are the eigenvalues of ρ^{T_2}. One can straightforwardly evaluate that the ideal NOON state Eq. (28) has a logarithmic negativity of $E = 1$. We note that this is not the maximal entanglement that the system can possess, the maximally entangled state takes a value $E_{\max} = \log_2(N+1)$ [38]. The reason for this is that the state Eq. (28) only involves two terms out of a possible $N+1$ terms in the superposition.

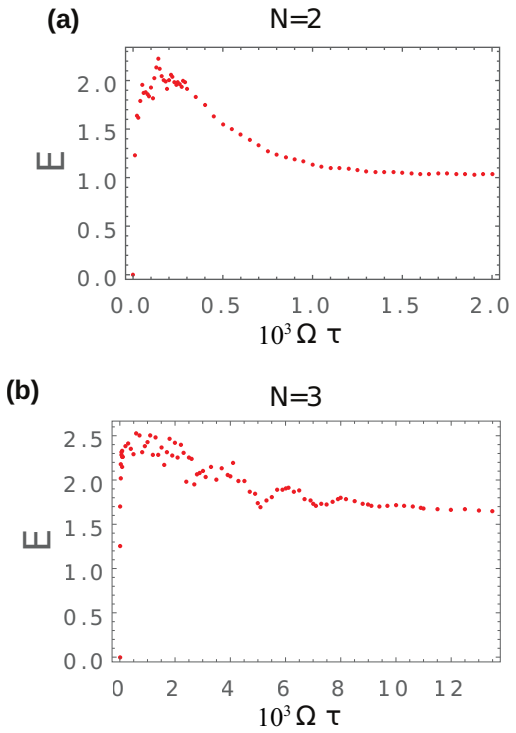

FIG. 5. Entanglement, as measured by the logarithmic negativity, for different pulse amplitudes and (a) $N = 2$, (b) $N = 3$. Parameters used are $\Delta t/\tau = 0.36$, $\Omega_r^{\max} = \Omega_e^{\max} = \Omega$, and $U\tau/\hbar = 2\Omega$.

In Fig. 5 we plot the entanglement generated as a function of the dimensionless pulse duration. We see that the entanglement stabilizes to a constant value for large $\Omega_{r,e}^{\max}\tau$, which is a direct result of adiabaticity. For small $\Omega_{r,e}^{\max}\tau$, the entanglement has some instability due to the nonadiabatic nature of the STIRAP pulses. This stabilizes to the adiabatic states as given by Eq. (33) for $N = 2$ and Eq. (27) for $N = 3$. The entanglement in the adiabatic limit grows with N due to the larger Hilbert space available. Interestingly, even in the nonadiabatic regime significant amounts of entanglement can be generated. In both cases examined, the entanglement quickly grows for very small STIRAP amplitudes, or equivalently very fast timescales $\Omega_{r,e}^{\max}\tau \sim 10$. This is due to the fact that in the nonadiabatic regime, the process is uncontrolled and might generate a different final state involving more states in the superposition, which would lead to more entanglement. Thus, while very large $\Omega_{r,e}^{\max}\tau$ is required for adiabaticity in particular for large N, from the point of view of entanglement generation, only a modest $\Omega_{r,e}^{\max}\tau$ should be necessary.

III. DOUBLE-STIRAP ENTANGLING GEOMETRIC PHASE GATE

We now describe a second method for producing entanglement between two BECs. In this scheme two STIRAP pairs are used instead of one, to produce a geometric phase gate between the states g_i and f_i (see Fig. 1). The state f_i could be represented by a hyperfine magnetic sublevel. The first STIRAP pair performs precisely the same operation as that described in the previous section. The role of the second STIRAP pair is to reverse the operation performed by the first STIRAP pair, so that the atoms are returned to the state g_i. In this scheme, the phase ϕ in Eq. (6) is nonzero. Using the definition Eq. (6) for the light pulse in the Hamiltonian Eq. (2), we can interpret this Hamiltonian in the rotating frame approximation, in which $\frac{d\phi}{dt}$ can be interpreted as a detuning. A phase is accumulated depending on the populations of g_1 and g_2, which gives rise to a entangling geometric phase gate. We again first review the qubit case originally presented in Refs. [34,35], then generalize to the BEC case.

A. Qubit case

In this section we show the scheme introduced in Refs. [34,35], which describes a method for entangling two atoms with a geometric phase gate. Let us consider again the configuration shown in Fig. 1, but consider a different initial state for the application of the STIRAP pulses, namely

$$|\psi(t=0)\rangle = \tfrac{1}{2}(|g_1\rangle + |f_1\rangle)(|g_2\rangle + |f_2\rangle), \tag{39}$$

which is an unentangled state. The STIRAP sequence that will be followed is showed in Fig. 1(c). The first STIRAP pair is identical to that discussed in Sec. IIA2. After some time, ΔT, defined as the difference in peak-to-peak times of the second pulse in each STIRAP, the reverse sequence is applied. Thus, after the whole sequence, the four states in Eq. (39) return to their initial state. However, a different phase may develop for each term in the superposition. The considerations of Sec. IIA1 and IIA2 immediately tell us the resulting transitions for each

of the states,

$$\begin{aligned}
&|f_1\rangle|f_2\rangle \rightarrow |f_1\rangle|f_2\rangle \rightarrow |f_1\rangle|f_2\rangle,\\
&|f_1\rangle|g_2\rangle \rightarrow e^{i\gamma_1'}|f_1\rangle|r_2\rangle \rightarrow e^{i\gamma_1}|f_1\rangle|g_2\rangle,\\
&|g_1\rangle|f_2\rangle \rightarrow e^{i\gamma_1'}|r_1\rangle|f_2\rangle \rightarrow e^{i\gamma_1}|g_1\rangle|f_2\rangle,\\
&|g_1\rangle|g_2\rangle \rightarrow e^{i\gamma_2'}(|e_1\rangle|e_2\rangle - |g_1\rangle|g_2\rangle) \rightarrow e^{i\gamma_2}|g_1\rangle|g_2\rangle,
\end{aligned} \tag{40}$$

where we have written the phase picked up after the first STIRAP pair as $\gamma_{1,2}'$ and the phase after the complete sequence as $\gamma_{1,2}$.

The final phases $\gamma_{1,2}$ may be calculated using the Berry formula [39],

$$\gamma = i\int_{\boldsymbol{R}_i}^{\boldsymbol{R}_f} \langle D|\nabla_{\boldsymbol{R}}|D\rangle \cdot d\boldsymbol{R}, \tag{41}$$

where $\boldsymbol{R} = (\theta,\phi)$ are the time varying parameters controlling the Hamiltonian and the integration is performed from the initial to final parameters $\boldsymbol{R}_{i,f}$, respectively. Note that there is no dynamical phase in the final states Eq. (40) as we work in the frame of reference such that the ground states g_i and f_i have zero phase evolution, and we also take the phase Eq. (5) to be zero.

To calculate γ_1 we take the dark state $|D\rangle$ to be Eq. (4), yielding [34]

$$\begin{aligned}
\gamma_1 &= -\int_{\phi_i}^{\phi_f} \sin^2\theta(t) d\phi\\
&= -\int_{t_i}^{t_f} \sin^2\theta(t)\frac{d\phi}{dt}dt.
\end{aligned} \tag{42}$$

In the pulse scheme that we consider in Fig. 1(c), in terms of the parameter $\theta(t)$, the evolution corresponds to $\theta(t) = 0 \rightarrow \pi/2 \rightarrow 0$. Therefore, in between the two STIRAP pairs, the integrand is $\sin^2\theta = 1$ and picks up a phase during the entire evolution. We may thus expect that approximately the phase $\gamma_1 \approx -\omega\Delta T$. Let us evaluate Eq. (42) under conditions such that $\phi(t) = \omega t$ and under the approximation that θ varies linearly in the region when both STIRAP pairs are on:

$$\theta(t) = \begin{cases} 0 & t \leqslant 0\\ \frac{\pi t}{2(\tau-\Delta t)} & 0 < t \leqslant \tau - \Delta t\\ \pi/2 & \tau - \Delta t < t \leqslant \Delta T\\ -\frac{\pi(t-\Delta T-\tau+\Delta t)}{2(\tau-\Delta t)} & \Delta T < t \leqslant \Delta T + \tau - \Delta t\\ 0 & t > \Delta T + \tau - \Delta t \end{cases}. \tag{43}$$

Under this approximation we can evaluate Eq. (42) exactly, leading to

$$\gamma_1 = -\omega\Delta T. \tag{44}$$

As expected, the dominant contribution to the integral Eq. (42) is during the time between the two STIRAP pairs when $\sin^2\theta = 1$ with duration ΔT. Meanwhile, for γ_2 we can substitute $|D_+\rangle$ in Eq. (8) into Eq. (41) to obtain

$$\gamma_2 = -2\int \frac{\cos^2\theta(t)\sin^2\theta(t)}{\cos^4\theta(t) + 2\sin^4\theta(t)}\frac{d\phi}{dt}dt. \tag{45}$$

In contrast to Eq. (42), the integrand of Eq. (45) is zero in between the two STIRAP pulses where $\theta = \pi/2$. This means that the only contribution to the integral is during the application of each STIRAP pair, not in between. Under the linear approximation Eq. (43) we may exactly evaluate Eq. (45) to give

$$\begin{aligned}
\gamma_2 &= \tfrac{2}{3}(-2+\sqrt{4+3\sqrt{2}})\omega(\tau-\Delta t)\\
&\approx -0.581\omega(\tau-\Delta t).
\end{aligned} \tag{46}$$

We see that γ_2 is independent of ΔT as expected since the integrand of Eq. (45) is zero during this time.

In the regime that $\omega\tau, \omega\Delta t \ll 1$, the Berry phase picked during the variation of the STIRAP pulses is negligible and we may set $\gamma_2 \approx 0$. Thus, the only contribution to the Berry phase is from γ_1, with the final state yielding

$$\begin{aligned}
&|\psi(t = \Delta T + \tau)\rangle\\
&\quad = \tfrac{1}{2}[(|f_1\rangle + e^{i\gamma_1}|g_1\rangle)|f_2\rangle + (e^{i\gamma_1}|f_1\rangle + |g_1\rangle)|g_2\rangle].
\end{aligned} \tag{47}$$

For $e^{i\gamma_1} = \pm i$, this is a maximally entangled state.

B. Generalizing to BEC case

As discussed in Sec. II B, explicit dark states for the BEC Hamiltonian Eq. (1) are difficult to obtain due to the multiboson nature of the problem. We may, however, deduce the effect of the geometric phase on BECs under certain limiting cases. Let us first obtain the dark state in the limits of $\theta = 0,\pi/2$ [i.e., only H_r or H_e is present respectively in Eq. (1)]. In Sec. II B 2 we considered the case where the atom numbers in each BEC N_i were the same. We now generalize this to the case when they are different, $N_1 \neq N_2$. We furthermore generalize this to the case when there is a nonzero population in the auxiliary f_i level.

First let us define the Fock states for a BEC when there is a population in the f_i level:

$$|k_i,n_i,\sigma_i\rangle_z = \begin{cases} \frac{(g_i^\dagger)^{k_i}(e_i^\dagger)^{n_i}(f_i^\dagger)^{N_i-k_i-n_i}}{\sqrt{k_i!n_i!(N_i-k_i-n_i)!}}|0\rangle & \text{if } \sigma_i = 0\\ \frac{(g_i^\dagger)^{k_i}(e_i^\dagger)^{n_i}(f_i^\dagger)^{N_i-k_i-n_i-1}}{\sqrt{k_i!n_i!(N_i-k_i-n_i-1)!}}|r_i\rangle & \text{if } \sigma_i = r \end{cases}, \tag{48}$$

where $f_i^\dagger$ is a bosonic creation operator for the state f_i with $i = 1,2$. In the limit when $\theta = 0$, only Hamiltonian H_r is present in Eq. (1). As this involves only the levels e_i and r_i, we may immediately write down a zero-energy eigenvalue state,

$$\sum_{k_1,k_2} \xi_{k_1k_2}|k_1,0,0\rangle_z|k_2,0,0\rangle_z, \tag{49}$$

where $k_i \in [0,N_i]$ and $\xi_{k_1k_2}$ are arbitrary coefficients as any superposition of a zero eigenvalue state also has zero eigenvalue. In the reverse limit of $\theta = \pi/2$, only Hamiltonian H_e is present in Eq. (1), giving the Hamiltonian Eq. (26). We may again write the eigenstates as

$$|k_i,n_i,\sigma_i\rangle_x = \begin{cases} \frac{(g_{x,i}^\dagger)^{k_i}(e_{x,i}^\dagger)^{n_i}(f_i^\dagger)^{N_i-k_i-n_i}}{\sqrt{k_i!n_i!(N_i-k_i-n_i)!}}|0\rangle & \text{if } \sigma_i = 0\\ \frac{(g_{x,i}^\dagger)^{k_i}(e_{x,i}^\dagger)^{n_i}(f_i^\dagger)^{N_i-k_i-n_i-1}}{\sqrt{k_i!n_i!(N_i-k_i-n_i-1)!}}|r_i\rangle & \text{if } \sigma_i = r \end{cases}, \tag{50}$$

The eigenvalues of these states are

$$S_i^x|k_i,n_i,\sigma_i\rangle_x = (k_i - n_i)|k_i,n_i,\sigma_i\rangle_x. \tag{51}$$

Let us consider how a typical dark state will evolve when changing parameters from $\theta = 0 \rightarrow \pi/2$. At the beginning

of the evolution with $\theta = 0$ let us focus on one term in the superposition Eq. (49),

$$|k_1,0,0\rangle_z |k_2,0,0\rangle_z. \tag{52}$$

Let us assume that $k_1 \leqslant k_2$, as the reverse case can be immediately written by interchanging labels $1 \leftrightarrow 2$. For the case that $k_1 + k_2$ is even, we may generalize Eq. (27) straighforwardly to give

$$\begin{aligned}&|D(\theta = 0 \to \pi/2); k_1 + k_2 = \text{even}\rangle \\ &= \sum_{k=0}^{k_1} \xi'_k |k, k_1 - k, 0\rangle_x \left| \frac{k_1 + k_2}{2} - k, \frac{k_2 - k_1}{2} + k, 0 \right\rangle_x ,\end{aligned} \tag{53}$$

where ξ'_k are arbitrary coefficients as all the terms in the superposition have zero eigenvalue. For $k_1 + k_2$ odd, we have

$$\begin{aligned}&|D(\theta = 0 \to \pi/2); k_1 + k_2 = \text{odd}\rangle \\ &= e^{i\phi(t)} \sum_{k=0}^{k_1 - 1} \xi'_k |k, k_1 - 1 - k, r\rangle_x \\ &\quad \times \left| \frac{k_1 + k_2 - 1}{2} - k, \frac{k_2 - k_1 + 1}{2} + k, 0 \right\rangle_x \\ &\quad + e^{i\phi(t)} \sum_{k=0}^{k_1} \xi''_k |k, k_1 - k, 0\rangle_x \\ &\quad \times \left| \frac{k_1 + k_2 - 1}{2} - k, \frac{k_2 - k_1 - 1}{2} + k, r \right\rangle_x ,\end{aligned} \tag{54}$$

where ξ'_k and ξ''_k are unspecified coefficients that are not necessary to calculate for our purposes. The fact that the above states are zero eigenvalue states may be verified by directly using the definition Eq. (51). The odd or even effect originates from the same origin as that for the single BEC case Eq. (25). The total spin Eq. (26) can only have zero eigenvalues for $k_1 + k_2$. For odd $k_1 + k_2$, a single Rydberg excitation remains reducing the total number of atoms in the g_i and e_i states by one, making the sum even. The phase factor $e^{i\phi(t)}$ follows from the fact that one can equally absorb this phase in the Hamiltonian Eq. (16) into the definition of the Rydberg state $|r_i\rangle \to e^{i\phi(t)}|r_i\rangle$. Then it follows that for each Rydberg excitation there is time-evolving phase $e^{i\phi(t)}$ in the dark state.

We may now use similar arguments to the previous section to estimate the Berry phase. Let us again consider the case that $\phi(t) = \omega t$ and the regime such that $\omega\tau, \omega\Delta t \ll 1$, so that there is negligible phase evolution during the STIRAP pairs. Then the dominant phase evolution occurs between the two STIRAP sequences, as for the qubit case. In this case, the only time-varying variable for the Berry phase is ϕ:

$$\gamma \approx i \int_0^{\Delta T} \langle D| \frac{\partial}{\partial \phi} |D\rangle \frac{d\phi}{dt} dt. \tag{55}$$

Substituting Eqs. (53) and (54), we obtain

$$\gamma = \begin{cases} 0 & k_1 + k_2 = \text{even} \\ -\omega\Delta T & k_1 + k_2 = \text{odd} \end{cases}. \tag{56}$$

We thus see that depending on whether the total number of atoms in the g_i states is odd or even, a phase is either picked up or not. We can see immediately that this is consistent with the qubit case Eq. (40), where a phase γ_1 is picked up on odd terms.

Let us now show that these phases lead to entanglement in the general case with $N_i > 1$. As a specific choice of Eq. (49) let us choose the initial state to be maximal $s_i^x = g_i^\dagger f_i + f_i^\dagger g_i$ eigenstates with respect to the levels g_i and f_i (not S_i^x which are with respect to the levels g_i and e_i):

$$\begin{aligned}&\frac{1}{\sqrt{N_1! N_2!}} \left(\frac{g_1^\dagger + f_1^\dagger}{\sqrt{2}} \right)^{N_1} \left(\frac{g_2^\dagger + f_2^\dagger}{\sqrt{2}} \right)^{N_2} |0\rangle \\ &= \frac{1}{\sqrt{2^{N_1+N_2}}} \sum_{k_1,k_2} \sqrt{\binom{N_1}{k_1}\binom{N_1}{k_2}} |k_1,0,0\rangle |k_2,0,0\rangle.\end{aligned} \tag{57}$$

Applying the rule Eq. (56) we obtain after the two STIRAP pulses the state

$$\begin{aligned}|D(\theta = 0 \to \pi/2 \to 0)\rangle &= \frac{1}{\sqrt{2^{N_1+N_2}}} \sum_{k_1,k_2} \sqrt{\binom{N_1}{k_1}\binom{N_1}{k_2}} \\ &\quad \times e^{i\omega\Delta T[(-1)^{k_1+k_2} - 1]/2} |k_1,0,0\rangle |k_2,0,0\rangle.\end{aligned} \tag{58}$$

This may be rewritten by putting the states in Schmidt form,

$$\begin{aligned}&|D(\theta = 0 \to \pi/2 \to 0)\rangle \\ &= e^{-i\omega\Delta T/2} \big[\cos(\omega\Delta T/2) \left|s_1^x = N_1\right\rangle \left|s_2^x = N_2\right\rangle \\ &\quad + i \sin(\omega\Delta T/2) \left|s_1^x = -N_1\right\rangle \left|s_2^x = -N_2\right\rangle \big],\end{aligned} \tag{59}$$

where

$$\begin{aligned}\left|s_i^x = \pm N_i\right\rangle &= \frac{1}{\sqrt{N_i!}} \left(\frac{g_i^\dagger \pm f_i^\dagger}{\sqrt{2}} \right)^{N_i} |0\rangle \\ &= \frac{1}{\sqrt{2^{N_i}}} \sum_{k_i=0}^{N_i} (\pm 1)^{k_i} \sqrt{\binom{N_1}{k_2}} |k_i,0,0\rangle.\end{aligned} \tag{60}$$

For $\omega\Delta T = \pi/2$, we can view Eq. (59) as a variant of a NOON state, as in terms of the occupation numbers of the states $\frac{g_i^\dagger + f_i^\dagger}{\sqrt{2}}$ the first term in Eq. (59) is N_1 and N_2, while the second terms are 0 and 0, respectively. An explicit form of the entanglement in Eq. (58) can be calculated using the logarithmic negativity Eq. (38). We obtain that the entanglement is for all N_1, N_2:

$$E = \log_2 \left[1 + \sqrt{\frac{1 - \cos(2\omega\Delta T)}{2}} \right]. \tag{61}$$

The entanglement is zero when $\omega\Delta T = n\pi$ and reaches a maximum at $2\omega\Delta T = (2n + 1)\pi$ for integer n.

C. Numerical analysis

In order to demonstrate the generation of entanglement, we simulate the adiabatic evolution using the same methods as that given in Sec. II C. The explicit form of the STIRAP pulses

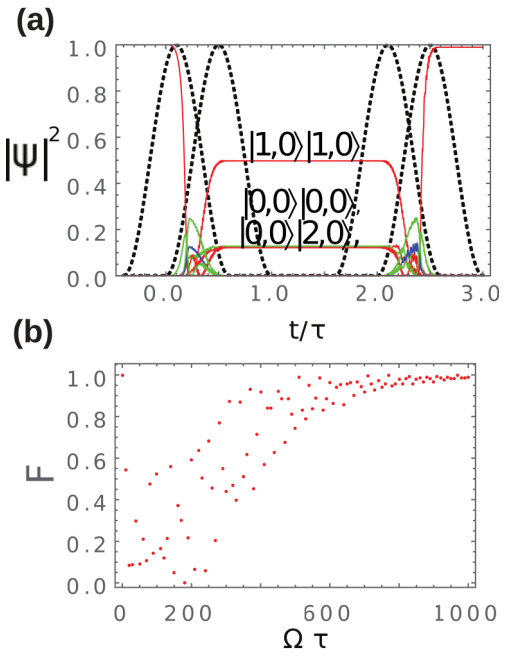

FIG. 6. (a) Typical time evolution for the geometric phase gate with two STIRAP sequences for $N_1 = N_2 = 2$ from the initial state $|k_1 = 0, r_1 = 0\rangle|k_2 = 0, r_2 = 0\rangle$. Parameters used are $\Delta t/\tau = 0.40$, $\Omega_r^{\max}\tau = 1000$, $\Omega_e^{\max}\tau = 1000$, $U\tau/\hbar = 2\Omega_e^{\max}$, $\omega\tau = -0.05$, and $\Delta T/\tau = 2$. (b) Fidelity of the initial state after the two STIRAP pulses for various values of $\Omega_r^{\max} = \Omega_e^{\max} = \Omega$.

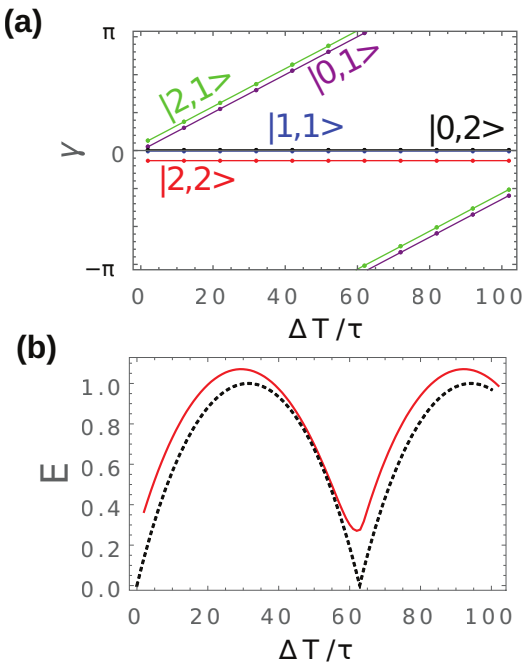

FIG. 7. (a) Phases picked up during two STIRAP pulse procedure by various states as labeled by $|k_1,k_2\rangle = |k_1,0,0\rangle_z|k_2,0,0\rangle_z$ in Eq. (49). The phases picked up by $|k_2,k_1\rangle$ are the same as $|k_1,k_2\rangle$. Parameters used are the same as in Fig. 6(a). Phases are with references to the state $|0,0\rangle$, which does not pick up any phase under the evolution. (b) Entanglement created by evolving the two STIRAP sequence starting from the state $|\frac{1}{\sqrt{2}},\frac{1}{\sqrt{2}}\rangle\rangle|\frac{1}{\sqrt{2}},\frac{1}{\sqrt{2}}\rangle\rangle$. Solid line shows the result for the phases picked up as in subfigure (a). Dashed lines shows the ideal result Eq. (60).

are

$$\Omega_e(t) = \begin{cases} \Omega_e^{\max}\sin^2\left(\frac{\pi t}{\tau}\right) & \text{if } 0 < t < \tau \\ \Omega_e^{\max}\sin^2\left(\frac{\pi(t-\Delta T+\Delta t)}{\tau}\right) & \\ \quad \text{if } \Delta T - \Delta t < t < \Delta T - \Delta t + \tau & \\ 0 \quad \text{otherwise} & \end{cases}, \tag{62}$$

and

$$\Omega_r(t) = \begin{cases} \Omega_e^{\max}\sin^2\left(\frac{\pi(t+\Delta t)}{\tau}\right) & \text{if } -\Delta t < t < \tau - \Delta t \\ \Omega_e^{\max} e^{-i\omega t}\sin^2\left(\frac{\pi(t-\Delta T)}{\tau}\right) & \text{if } \Delta T < t < \tau + \Delta T \\ 0 & \text{otherwise} \end{cases}. \tag{63}$$

The first STIRAP pair is identical to Eqs. (30) and (31), and the second pair occurs a time ΔT later, but in the reverse order as the first. As the level f_i takes no part in the Hamiltonian Eq. (15), we take this into account implicitly, by evolving the same Eq. (29) as for the single STIRAP pair sequence. We time evolve each term in the superposition Eq. (57) separately and examine what phase is obtained on the final state.

Figure 6(a) shows the population evolution for typical parameters. We see that for sufficiently large $\Omega_{r,e}^{\max}\tau$ the curves follow an adiabatic path, such that it returns to the initial state at the end of the evolution, with the first half of the evolution being identical to Fig. 3. Figure 6(b) shows the fidelity of the transfer from various initial states Eq. (52) before and after the geometric phase evolution. Here the fidelity is defined as

$$F = |(\langle k_1 = 0, r_1 = 0 \otimes |\langle k_2 = 0, r_2 = 0|)|\psi(t)\rangle|^2. \tag{64}$$

We see that as before, increasing $\Omega_{e,g}^{\max}\tau$ improves the fidelity, as the system is able to maintain adiabaticity. In the nonadiabatic regime the return to the initial state is rather uncontrolled, which gives rise to the noisy behavior [Fig. 6(b)]. We note the time evolution is completely deterministic, but the complex nonadiabatic behavior gives a fast dependence with Ω.

In Fig. 7(a) we plot the phase that each of the states in Eq. (49) acquires after the geometric gate sequence. We see that as a function of ΔT there is a linear relation to the phase that is obtained on states with odd $k_1 + k_2$, as expected from Eq. (56). The gradient of the phase with ΔT agrees well with Eq. (56), giving a value close to ω. For even $k_1 + k_2$ the phase variation with ΔT is completely flat, in agreement with Eq. (56). The deviation from zero phase for even states is attributed to the approximations that were assumed in Eq. (56), namely that $\omega\tau, \omega\Delta T$ are negligible. In practice we see that due to the lack of variation of the even terms with ΔT this provides an offset to the relative phase between the odd and even terms.

Figure 7(b) shows the entanglement as quantified by the logarithmic negativity Eq. (38) after starting in the state Eq. (57). We directly see that entanglement can be created using the geometric gate sequence. The general behavior has good agreement with the theory Eq. (61). We see that the entanglement does not reach zero in the simulations in contrast

to the theory. We also see a slight offset of the periodicity of the entanglement curves for the numerically evolved case, in comparison to the theory. The reason for this is due to the phases of each of the states involved in the states as shown in Fig. 7(a) not all giving zero at the end of the double STIRAP evolution. This again is attributed to the assumptions made in deriving Eq. (61) breaking down. Specifically, the finite $\omega\tau$,$\omega\Delta T$ adds a phase on the even $k_1 + k_2$ terms, which offsets the maximally entangled point. This added phase contributes to the entanglement, which can account for the fact that the simulation plot achieves a higher entanglement than the ideal case.

IV. SUMMARY AND CONCLUSIONS

We have shown two methods of generating entangled states between two BECs using Rydberg excitations. In the first method, one STIRAP sequence where a Rydberg state is produced in each BEC results in a state of the form

$$\sum_{k=0}^{N} \xi_k |k\rangle_x |N-k\rangle_x, \tag{65}$$

where $\xi_k = \xi_{N-k}$ we label the occupation of an S^x eigenstate between the levels g_i and e_i and have omitted the Rydberg labels that are unoccupied. In the second method, two STIRAP pulses result in a geometric phase gate, which result for suitable parameters

$$\cos\left(\frac{\omega\Delta}{2}\right)|N\rangle'_x|N\rangle'_x + i\sin\left(\frac{\omega\Delta}{2}\right)|0\rangle'_x|0\rangle'_x, \tag{66}$$

where $|N\rangle'_x$,$|0\rangle'_x$ denotes the full or zero occupation of the $s^x = N$ state between the g_i and f_i levels as defined in Eq. (60), respectively. This is a variation of a NOON state, and can be explicitly written as a NOON state if we define the s^x eigenstates in the opposite way on the two BECs. The primary advantage of the geometric phase gate is that the type of states that can be produced are tunable using the delay ΔT between the STIRAP pulses. The single-STIRAP sequence does not have a tunable parameter, hence only the equal superposition state Eq. (65) can be produced. The price to be paid for this tunability is a more complex STIRAP sequence.

Both schemes result in entanglement between the BECs. The single STIRAP sequence has entanglement of the order of $E \sim \log_2(N+1)$, due to the nature of the entangled state Eq. (65) created. This is the state produced in the adiabatic limit, which is likely to be rather challenging to reach for the large BECs, due to the larger number of states involved. We have, however, found that even in the nonadiabatic limit large amounts of entanglement are created, which in fact exceed the adiabatic case. This occurs on very short timescales, $\Omega\tau \sim 10$, according to the cases that we simulated, hence this may be experimentally advantageous. One aspect of this approach is that the type of state produced is not particularly well controlled for the single-STIRAP case, as the parameters ξ_k are arbitrary, up to symmetrization. Nevertheless, this consistently produces entanglement and is guaranteed to exist in the adiabatic case.

For the double-STIRAP case, a NOON state is generated independent of N_1,N_2. The amount of entanglement in this case is at most $E = 1$, as shown by Eq. (61). Therefore, the single-STIRAP sequence has a larger amount of entanglement as N increases. On the other hand, the type of state is better controlled, and in the adiabatic limit is of form which is a more familiar form. A NOON state is well-known to have beneficial properties from the point of view of quantum metrology. However, this requires rather large $\Omega\tau$ to maintain adiabaticity, particularly for large N, and is likely to be challenging experimentally to produce.

One of the main attractive aspects of using the STIRAP methods and Rydberg excitations is the suppression of spontaneous emission due to long lifetimes and long-ranged interactions. In this paper we were concerned more with the fundamental scheme of extending the single atom methods to BECs, which makes a direct analytical solution of the dark states a nontrivial task. In an experimental setting it is possible to adapt our methods to make them more advantageous in terms of spontaneous emission using a more complex excitation path to suppress these effects. For the single-atom case, this has been discussed in detail in Refs. [34,35]. These should be directly also applicable to the BEC case. Another direction that was not considered is how well our scheme is robust in the presence of decoherence for our particular scheme. A common problem of NOON states in any physical system is their sensitivity to decoherence for large particle numbers. In a typical BEC on atom chips there can be in the region of $N = 10^3$ atoms, hence the effects of accelerated decoherence can be considerable [38], although excellent coherent times for BECs in the region of seconds have been observed [40]. As NOON states are very sensitive in the presence of decoherence, it is likely the single-STIRAP scheme is more robust experimentally, in view of the shorter pulses required and the type of state generated. Alternatively, "kitten" NOON states could be targeted with the double-STIRAP sequence, provided the atom numbers in each BEC can be precisely controlled.

ACKNOWLEDGMENTS

T.B. acknowledges the support of NTT Basic Research Laboratories, the Shanghai Research Challenge Fund, and National Natural Science Foundation of China Grant No. 61571301. R.S. acknowledges financial support by the EU H2020 FET Proactive project RySQ (No. 640378), the Marie Curie Initial Training Network COHERENCE (No. 265031), and by the Foundation for Fundamental Research on Matter (FOM), which is part of the Netherlands Organization for Scientific Research (NWO).

[1] S. Stenholm and K. Suominen, *Quantum Approach to Informatics* (Wiley, New York, 2005).

[2] T. D. Ladd, F. Jelezko, R. Laflamme, Y. Nakamura, C. Monroe, and J. L. OBrien, Nature **464**, 45 (2010).

[3] P. Schindler, D. Nigg, T. Monz, J. T. Barreiro, E. Martinez, S. X. Wang, S. Quint, M. F. Brandl, V. Nebendahl, C. F. Roos *et al.*, New J. Phys. **15**, 123012 (2013).
[4] Y. Nakamura, Y. A. Pashkin, and J. S. Tsai, Nature (London) **398**, 786 (1999).
[5] C. Adami and N. Cerf, in *Quantum Computing and Quantum Communications*, edited by C. Williams (Springer, Berlin/Heidelberg, 1999), Vol. 1509 of Lecture Notes in Computer Science, pp. 391–401.
[6] D. Loss and D. P. DiVincenzo, Phys. Rev. A **57**, 120 (1998).
[7] M. V. G. Dutt, L. Childress, L. Jiang, E. Togan, J. Maze, F. Jelezko, A. S. Zibrov, P. R. Hemmer, and M. D. Lukin, Science **316**, 1312 (2007).
[8] B. Julsgaard, A. Kozhekin, and E. S. Polzik, Nature **413**, 400 (2001).
[9] D. Matsukevich, Nature Phys. **9**, 389 (2013).
[10] X.-H. Bao, X.-F. Xu, C.-M. Li, Z.-S. Yuan, C.-Y. Lu, and J.-W. Pan, Proc. Natl. Acad. Sci. USA **109**, 20347 (2012).
[11] H. Imai, K. Inaba, H. Tanji-Suzuki, M. Yamashita, and T. Mukai, Appl. Phys. B **116**, 821 (2014).
[12] P. Bohi, M. F. Riedel, J. Hoffrogge, J. Reichel, G. J. Milburn, J. Corney, T. W. Hansch, and P. Treutlein, Nat. Phys. **5**, 592 (2009).
[13] M. F. Riedel, P. Bohi, L. Yun, T. W. Hnsch, A. Sinatra, and P. Treutlein, Nature **464**, 1170 (2010).
[14] S. Tojo, Y. Taguchi, Y. Masuyama, T. Hayashi, H. Saito, and T. Hirano, Phys. Rev. A **82**, 033609 (2010).
[15] V. Y. F. Leung, D. R. M. Pijn, H. Schlatter, L. Torralbo-Campo, A. L. La Rooij, G. B. Mulder, J. Naber, M. L. Soudijn, A. Tauschinsky, C. Abarbanel *et al.*, Rev. Sci. Instrum. **85**, 053102 (2014).
[16] V. Y. F. Leung, A. Tauschinsky, N. van Druten, and R. J. C. Spreeuw, Quant. Info. Proc. **10**, 955 (2011).
[17] A. Abdelrahman, T. Mukai, H. Häffner, and T. Byrnes, Opt. Express **22**, 3501 (2014).
[18] I. Herrera, Y. Wang, P. Michaux, D. Nissen, P. Surendran, S. Juodkazis, S. Whitlock, R. J. McLean, A. Sidorov, M. Albrecht *et al.*, J. Phys. D: Appl. Phys. **48**, 115002 (2015).
[19] S. Jose, P. Surendran, Y. Wang, I. Herrera, L. Krzemien, S. Whitlock, R. McLean, A. Sidorov, and P. Hannaford, Phys. Rev. A **89**, 051602 (2014).
[20] H. Kurkjian, K. Pawłowski, A. Sinatra, and P. Treutlein, Phys. Rev. A **88**, 043605 (2013).
[21] T. F. Viscondi, K. Furuya, and M. C. de Oliveira, Europhys. Lett. **90**, 10014 (2010).
[22] L. Ya-Feng, Z. Xu-Bo, and G. Guang-Can, Commun. Theor. Phys. **62**, 13 (2014).
[23] A. N. Pyrkov and T. Byrnes, New J. Phys. **15**, 093019 (2013).
[24] D. Rosseau, Q. Ha, and T. Byrnes, Phys. Rev. A **90**, 052315 (2014).
[25] J. Esteve, C. Gross, A. Weller, S. Giovanazzi, and M. Oberthaler, Nature **455**, 1216 (2008).
[26] T. Berrada, S. van Frank, R. Bücker, T. Schumm, J.-F. Schaff, and J. Schmiedmayer, Nature Communications **4**, 2077 (2013).
[27] W. Muessel, H. Strobel, D. Linnemann, D. B. Hume, and M. K. Oberthaler, Phys. Rev. Lett. **113**, 103004 (2014).
[28] T. Byrnes, K. Wen, and Y. Yamamoto, Phys. Rev. A **85**, 040306 (2012).
[29] H. Cable, F. Laloë, and W. J. Mullin, Phys. Rev. A **83**, 053626 (2011), .
[30] A. N. Pyrkov and T. Byrnes, Phys. Rev. A **90**, 062336 (2014).
[31] T. G. Walker and M. Saffman, in *Advances in Atomic, Molecular, and Optical Physics*, edited by E. A. Paul Berman and C. Lin (Academic Press, San Diego, 2012), Vol. 61 of Advances In Atomic, Molecular, and Optical Physics, pp. 81–115.
[32] R. Heidemann, *Rydberg Excitation of Bose-Einstein Condensates: Coherent Collective Dynamics* (Verlag, Berlin, 2008).
[33] I. I. Beterov, M. Saffman, E. A. Yakshina, V. P. Zhukov, D. B. Tretyakov, V. M. Entin, I. I. Ryabtsev, C. W. Mansell, C. MacCormick, S. Bergamini *et al.*, Phys. Rev. A **88**, 010303 (2013).
[34] D. Møller, Adiabatic Processes in Quantum Computation: Experimental and Theoretical Studies, Ph.D. thesis, Department of Physics and Astronomy, University of Aarhus, 2008.
[35] D. Møller, L. B. Madsen, and K. Mølmer, Phys. Rev. Lett. **100**, 170504 (2008).
[36] G. Günter, M. Robert-de Saint-Vincent, H. Schempp, C. S. Hofmann, S. Whitlock, and M. Weidemüller, Phys. Rev. Lett. **108**, 013002 (2012).
[37] B. Olmos, W. Li, S. Hofferberth, and I. Lesanovsky, Phys. Rev. A **84**, 041607 (2011).
[38] T. Byrnes, Phys. Rev. A **88**, 023609 (2013).
[39] M. V. Berry, Proc. R. Soc. London A **392**, 45 (1984).
[40] P. Treutlein, T. Steinmetz, Y. Colombe, B. Lev, P. Hommelhoff, J. Reichel, M. Greiner, O. Mandel, A. W. T. Rom, I. Bloch *et al.*, Fortschr. Phys. **54**, 702 (2006).